

# Circular L-RNA aptamer promotes target recognition and controls gene activity

Danyang Ji<sup>1</sup>, Kaixin Lyu<sup>1</sup>, Haizhou Zhao<sup>1</sup> and Chun Kit Kwok<sup>1,2,\*</sup>

<sup>1</sup>Department of Chemistry and State Key Laboratory of Marine Pollution, City University of Hong Kong, Kowloon Tong, Hong Kong SAR, China and <sup>2</sup>Shenzhen Research Institute of City University of Hong Kong, Shenzhen, China

Received April 06, 2021; Revised June 22, 2021; Editorial Decision June 24, 2021; Accepted June 28, 2021

## ABSTRACT

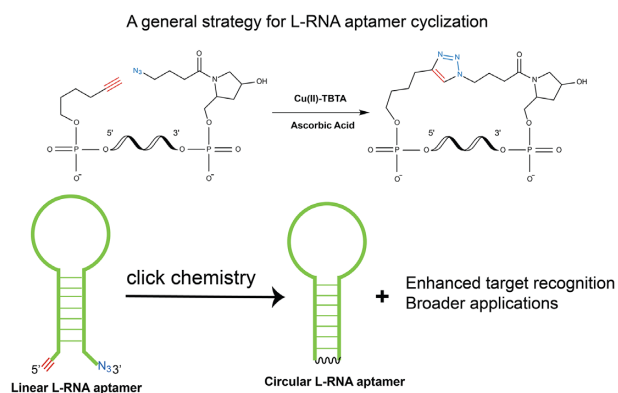
**Rational design of aptamers to incorporate unnatural nucleotides and special chemical moieties can expand their functional complexity and diversity. Spiegelmer (L-RNA aptamer) is a unique class of aptamer that is composed of unnatural L-RNA nucleotides, and so far there are limited L-RNA aptamer candidates and applications being reported. Moreover, the target binding properties of current L-RNA aptamers require significant improvement. Here, using L-Apt.4-1c as an example, we develop a simple and robust strategy to generate the first circular L-RNA aptamer, cycL-Apt.4-1c, quantitatively, demonstrate substantial enhancement in binding affinity and selectivity toward its target, and notably report novel applications of circular L-RNA aptamer in controlling RNA–protein interaction, and gene activity including telomerase activity and gene expression. Our approach and findings will be applicable to any L-RNA aptamers and open up a new avenue for diverse applications.**

## INTRODUCTION

DNA or RNA aptamers fold into specific secondary and/or tertiary structures to recognize a variety of targeted molecules (1–4). The superior properties of aptamer compared to traditional protein-based antibodies, including but not limited to the ability to bind to a broad range of targets, automated and scalable DNA/RNA synthesis, ease of aptamer modification and functionalization, flexibility and versatility in the design of apta-sensors, made them attractive candidates for diagnostic and therapeutic applications (4–7). Nevertheless, unmodified nucleic acid aptamers are unstable in biological fluids and rapidly degraded by nucleases, which limited their applications (8,9). To address this, nuclease-resistant aptamers with chemical modifications, such as  $\alpha$ -L-threose nucleic acid (TNA) aptamer, 2'-O-methyl aptamer, and locked nucleic acid (LNA) aptamer have been developed (10–14). These modifications, if made after selection process, can potentially affect the binding properties of aptamers (15–17). Another strategy is the development of L-RNA aptamers (18–22). Recently, our group have reported the first 2 L-RNA aptamers, namely L-Ap3-7 and L-Apt.4-1c (23,24), that target RNA G-quadruplex structure, a non-canonical nucleic acids motif of biological significance (25–28).

L-RNA aptamers (or Spiegelmers) are composed of unnatural L-RNA nucleotides, and not able to hybridize with natural D-RNA through Watson–Crick base-pairing (29). Given their unnatural nature, L-RNA aptamers are resistant to nucleases degradation, which make them biostable and well-suited for biological and biomedical applications (30,31). Despite the potential applications, so far L-RNA aptamers have not achieved widespread use. One of the major problems is that there are limited modification and optimization approaches to improve the target recognition properties of L-RNA aptamers, such as conformational stability, binding affinity and specificity. In particular, conformational stability is a significant factor for the successful use of aptamers in complex conditions. Although the conformational flexibility enables the aptamers to recognize targets, the flexible regions are also exposed to non-targets and can cause off-target interactions (32,33). In addition,

## GRAPHICAL ABSTRACT



\*To whom correspondence should be addressed. Tel: +852 3442 6858; Fax: +852 3442 0522; Email: ckkwok42@cityu.edu.hk

the flexible conformation may misfold in human serum or cell where there are lower concentrations of  $Mg^{2+}$  and  $Ca^{2+}$  to maintain the tertiary structure of aptamers (34). Therefore, new chemistries that modulate L-RNA aptamer structure for enhanced stability, binding affinity and specificity are highly desired.

Studies on cyclization of natural nucleic acid have revealed that circular structures possess better thermal stability and increased conformational stability owing to the lack of free ends and reduction in misfolding (35–37). Among the various chemical- or enzymatic-based cyclization methods, click chemistry reaction can provide a simple method to ligate nucleic acid molecules with high efficiency at mild reaction conditions (38,39). The copper(I)-catalyzed azide-alkyne cycloaddition (CuAAC) is the best example for this kind of reactions (36,38). Azide and alkyne groups can generally be introduced to nucleic acids easily without affecting their biophysical properties. Thus, we hypothesize that click cyclization can provide a simple and efficient strategy to improve the diversity and performance of unnatural L-RNA aptamers. Recently, our group have developed L-Apt.4-1c, a linear L-RNA aptamer targeting human telomerase RNA G-quadruplex (*hTERC* D-rG4), and demonstrated its inhibition on *hTERC* rG4-nucleolin interactions (24). However, the potential applications of L-Apt.4-1c, especially in complex environment or in cells, has not been fully studied and explored due to the limitations on binding affinity and stability. To substantially improve this, herein we rationally design the L-Apt.4-1c aptamer construct and chemically ligate the 5' and 3' terminals of L-Apt.4-1c through intramolecular CuAAC reaction with high efficiency and develop the first chemically cyclized L-RNA aptamer (cycL-Apt.4-1c) (Figure 1). CycL-Apt.4-1c exhibits stronger binding affinity, better specificity, and higher conformational stability than linear L-Apt.4-1c. Competitive binding assay with protein, telomerase repeated amplification protocol (TRAP) assay and dual luciferase reporter gene assay further validated the promising applications of cycL-Apt.4-1c in *in vitro* and in cells for the first time.

## MATERIAL AND METHODS

### Materials

All the L-RNA oligonucleotides with the sequences listed in Supplementary Table S1 were synthesized and characterized by Bio-Synthesis Inc (USA). All the D-RNA and D-DNA oligonucleotides listed in Supplementary Table S1 were synthesized by Integrated DNA Technologies Inc. (USA) and Genewiz Biotechnology Co., Ltd. (Suzhou, China), respectively. The ESI mass spectrum of cycL-Apt.4-1c was characterized by Genewiz Biotechnology Co., Ltd. (Suzhou, China). Cu(II)-TBTA (Tris((1-benzyl-4-triazolyl)methyl)amine) complex in 55% aq. DMSO (10 mM) was bought from Lumiprobe Corporation (USA). L (+)-Ascorbic acid and urea were purchased from Acros Organics (USA). Thioflavin T (ThT) was ordered from Solarbio Life Science (Beijing, China). SYBR Gold nucleic acid gel stain, D-Sucrose, potassium chloride (KCl) solution (3 M), RNase A, fetal bovine serum (FBS) and Lipofectamine® 2000 were ordered from Thermo Fisher Scientific (USA). Magnesium chloride ( $MgCl_2$ ) solution

(1 M) and NaOH solution (10 M) were bought from Sigma-Aldrich (USA). Potassium acetate (KAc) was purchased from J&K Scientific Co., Ltd. (Beijing, China). DHX36 protein was synthesized by OriGene Technologies Inc. (USA). TRAPeZe® Telomerase Detection Kit (Merck Millipore, USA) was used for TRAP assays. PsiCHECK-2 vector (Promega, USA) and Dual-Luciferase Reporter Assay kit (Promega, USA) were used in reporter gene assays. RNase Plus Mini Kit (Qiagen, Germany), SuperScript III reverse transcriptase (Thermo Fisher Scientific, USA), random Primers (Thermo Fisher Scientific, USA) and SsoAdvanced Universal SYBR Green Supermix (Bio-Rad, USA) were used in qRT-PCR tests. All the stocks and buffers were prepared using nuclease-free ultrapure distilled water (Thermo Fisher Scientific, USA).

### Methods

#### *Cyclization of L-Apt.4-1c using click chemistry reaction.*

The click reaction was performed based on the previously reported method with further optimization (36). The 5'-alkyne and 3'-azide labeled L-Apt.4-1c was synthesized by company. We have chosen 5'-alkyne and 3'-azide due to its cheaper cost and easier synthesis as compared to other options for click cyclization, and in our hands this option yields >95% as shown in Figure 2. One may also choose different combination or orientation of functional groups according to their specific application and requirement. The oligonucleotide was dissolved by nuclease-free ultrapure distilled water to get a stock solution of 100  $\mu$ M. L-Apt.4-1c (500 nM) was denatured at 95°C for 3 min in Tris-HCl buffer (25 mM Tris-HCl, 50 mM KCl, and 5 mM  $MgCl_2$ , pH 7.5) and then quickly cooled down on ice before cyclization. Under the optimized condition, 25  $\mu$ M Cu(II)-TBTA and 250  $\mu$ M freshly prepared ascorbic acid were added to L-Apt.4-1c. The click chemistry reaction was carried out at 37°C for 2 h. The reaction solution was desalted using Zymo-Spin IC Columns and analyzed on 12% denaturing polyacrylamide gel (PAGE) with SYBR Gold staining. The same procedures were also used for D-Apt.4-1c cyclization.

#### *Fluorescence detection of cycL-Apt.4-1c/L-Apt.4-1c with ThT.*

Fluorescence detection was performed on a HORIBA FluoroMax-4 fluorescence spectrophotometer (Japan) using 1-cm path length quartz cuvette. CycL-Apt.4-1c (or L-Apt.4-1c) (300 nM) was heated at 95°C for 3 min and cooled down on ice for 10 min before use. ThT (2  $\mu$ M) was mixed with cycL-Apt.4-1c (or L-Apt.4-1c) in Tris-HCl buffer (25 mM Tris-HCl, 150 mM KCl/LiCl, and 1 mM  $MgCl_2$ , pH 7.5). The samples were incubated at room temperature for 30 min followed by fluorescence measurement. Spectra of ThT were excited at 425 nm and scanned from 450 nm to 600 nm. Excitation and emission slits were set at 5 nm.

#### *Circular dichroism (CD) spectroscopy.*

CD spectra were recorded on a Jasco CD J-150 spectrometer with 1-cm path length quartz cuvette. CycL-Apt.4-1c (or L-Apt.4-1c) (500 nM) in Tris-HCl buffer (25 mM Tris-HCl, 150 mM KCl/LiCl, and 1 mM  $MgCl_2$ , pH 7.5) was heated at 95°C for 3 min and cooled down on ice for 10 min before CD

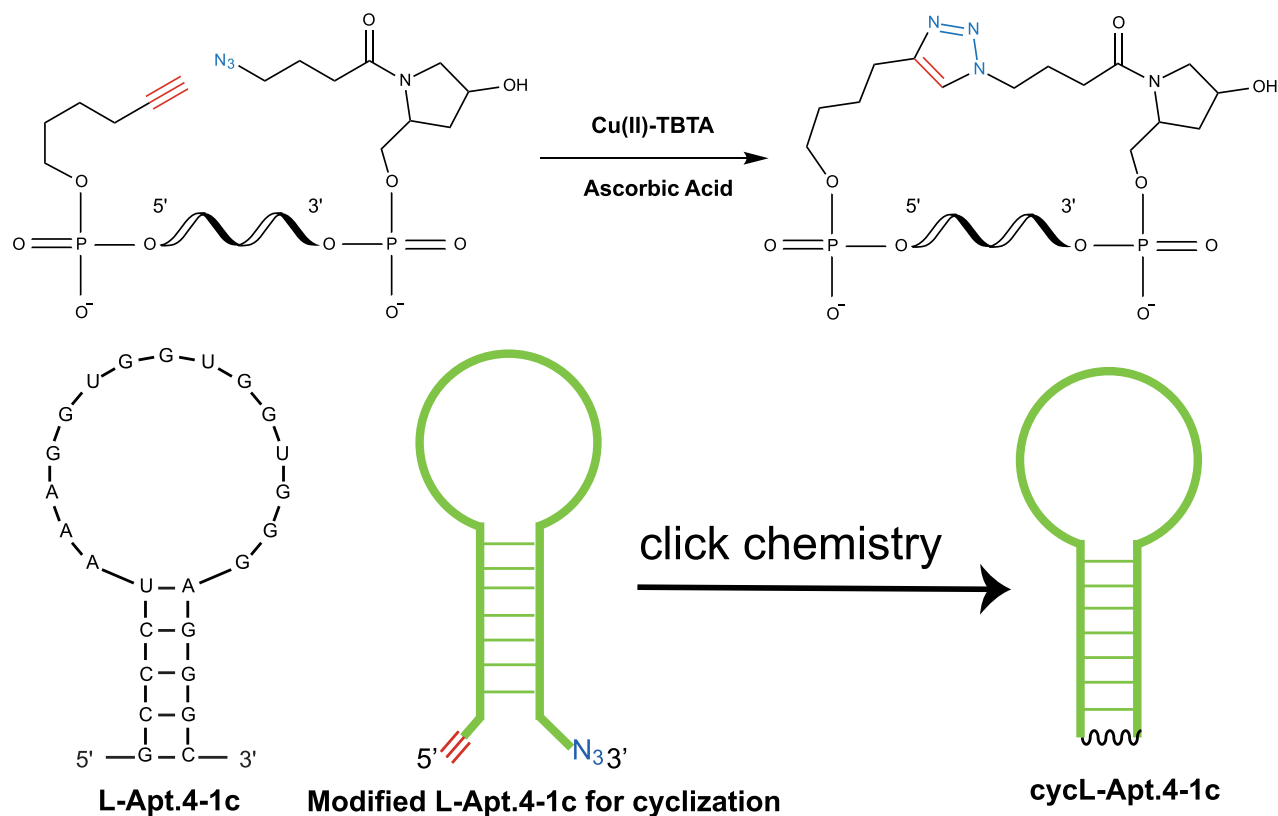


**Figure 1.** Schematic representation of the preparation of cyclL-Apt.4-1c. Alkyne and azide residues are introduced at the 5' and 3' end of linear L-Apt.4-1c aptamer construct for CuAAC reaction. Cu(II)-TBTA and ascorbic acid are used in the click reaction to catalyze the cyclization.

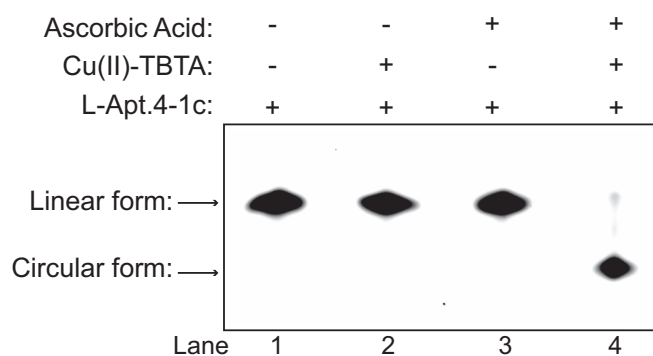


**Figure 2.** Cyclization of L-Apt.4-1c using click chemistry. Denaturing gel shows cyclization result of linear L-Apt.4-1c to circular L-Apt.4-1c under the optimal concentrations of ascorbic acid and Cu(II)-TBTA.

measurements. Three scans from 220 to 310 nm at 1 nm intervals were accumulated and averaged.

**Electrophoretic mobility shift assay (EMSA).** CyclL-Apt.4-1c was heated at 75°C for 3 min and cooled down at room temperature for 10 min before use. FAM-labeled *hTERC* D-rG4 (30 nM) was mixed with different concentrations of cyclL-Apt.4-1c (0–200 nM) in Tris-HCl buffer (25 mM Tris-HCl, 150 mM KCl and 1 mM MgCl<sub>2</sub>, pH 7.5), and incubated at 37°C for 30 min. Sucrose (8%) was added to samples before loading onto a 12% native PAGE

(19:1, acrylamide:bis-acrylamide). The gel was prepared with Tris-HCl buffer (25 mM Tris-HCl, 50 mM KAC and 1 mM MgCl<sub>2</sub>, pH 7.5), which was also used as running buffer. The electrophoresis was carried out at 4°C for 50 min with a consistent current at 70 mA. The gel was scanned by FujiFilm FLA-9000 Gel Imager at 650 V and quantified by ImageJ. The binding curve was fitted by Graphpad Prism using the one site-specific binding model. Three replicates were performed for each concentration and the standard deviation of them was calculated as error bar. The same procedures were also used for the other binding tests in this work.

**Microscale thermophoresis (MST) assay.** CyclL-Apt.4-1c was heated at 75°C for 3 min and cooled down at room temperature for 10 min before use. FAM-labeled *hTERC* D-rG4 (100 nM) was mixed with different concentrations of cyclL-Apt.4-1c (0–2 μM) in Tris-HCl buffer (25 mM Tris-HCl, 150 mM KCl and 1 mM MgCl<sub>2</sub>, pH 7.5), and incubated at 37°C for 30 min and subsequently applied to MST assay. MST assays were carried out on a Monolith NT.115 instrument (NanoTemper, Munich, Germany) using the 'nanoblu' channel. Data were fitted by NanoTemper Analysis with a  $K_d$  model from the MST machine. Three replicates were performed for each concentration and the standard deviation of them was calculated as error bar. The same procedures were also used for the MST tests of other oligos in this work.

**Specificity test of *cycL-Apt.4-1c* to *hTERC D-rG4*.** FAM-labeled *hTERC D-rG4* (30 nM) and other DNA/RNA oligos (30 nM) listed in Supplementary Table S1 were mixed with 100 nM of pre-annealed *cycL-Apt.4-1c* in Tris-HCl buffer (25 mM Tris-HCl, 150 mM KCl, and 1 mM MgCl<sub>2</sub>, pH 7.5). Then the samples were incubated at 37°C for 30 min. After that, sucrose (8%) was added and samples were loaded to a 12% native PAGE. The performing and analysis procedure of PAGE were the same as EMSA section.

**Stability tests.** The stability of *cycL-Apt.4-1c* in urea was analyzed by 12% native PAGE (19:1, acrylamide:bis-acrylamide). The gel was prepared with Tris-HCl buffer (25 mM Tris-HCl, 50 mM KAC and 1 mM MgCl<sub>2</sub>, pH 7.5), which was also used as running buffer. Pre-annealed *cycL-Apt.4-1c* (100 nM) or *L-Apt.4-1c* (100 nM) were mixed with 500 mM, 1 M, 2 M and 5 M urea in Tris-HCl buffer (25 mM Tris-HCl, 150 mM KCl and 1 mM MgCl<sub>2</sub>, pH 7.5) and incubated at 37°C for 30 min. Then the samples were loaded to gel with sucrose (8%). The electrophoresis was carried out at room temperature for 30 min with a consistent current at 70 mA followed by SYBR Gold staining.

The stability of *cycL-Apt.4-1c* against RNase A, FBS, cell lysate and NaOH solution was analyzed by 12% denaturing PAGE containing 8 M urea and 1× Tris borate EDTA (TBE) buffer. *CycL-Apt.4-1c* (100 nM) was mixed with 100 ng/μl of RNaseA, 5% FBS, HEK293T cell lysate (600 cell/ul) and NaOH solution (1 and 100 mM), respectively. The samples were incubated at room temperature for 0 to 120 min and analyzed by denaturing PAGE with SYBR Gold staining. The stability tests of *L-Apt.4-1c* against RNase A, FBS and cell lysate were performed with the same procedures as that of *cycL-Apt.4-1c*.

**Competitive inhibition of *hTERC D-rG4-DHX36* binding by *cycL-Apt.4-1c*.** FAM-labeled *hTERC D-rG4* (30 nM) was mixed with different concentrations of *cycL-Apt.4-1c* (0–1 μM) and fixed amount of *DHX36* (100 nM) in Tris-HCl buffer (25 mM Tris-HCl, 150 mM KCl, and 1 mM MgCl<sub>2</sub>, pH 7.5). The mixtures were incubated at 37°C for 30 min and loaded to a 8% native PAGE (37.5:1, acrylamide:bis-acrylamide). The gel was prepared with Tris-HCl buffer (25 mM Tris-HCl, 50 mM KAC and 1 mM MgCl<sub>2</sub>, pH 7.5), which was also used as running buffer. Then the gel was performed at 70 mA for 30 min. Inhibition curve of *cycL-Apt.4-1c* on *hTERC D-rG4-DHX36* complex formation was fitted by Graphpad Prism using the dose-response inhibition model. IC<sub>50</sub> value was calculated using the log[*cycL-Apt.4-1c*] and normalized response. Three replicates were performed for each concentration and the standard deviation of them was calculated as error bar.

**Telomerase repeated amplification protocol (TRAP) assay.** According to the manufacturer of the TRAPEZE<sup>®</sup> gel-based telomerase detection kit, a three-step TRAP procedure was performed: (i) addition of telomeric repeats to the telomerase substrate by telomerase, (ii) amplification of telomerase product by PCR, (iii) detection of telomerase products by electrophoresis. HEK293T cell extracts were prepared first using the CHAPS lysis buffer provided by the kit. Under best conditions, cell extracts from 500 cells

were mixed with different concentrations of pre-annealed *cycL-Apt.4-1c* (0–8 μM) (or other control oligos/ligands) in Tris-HCl buffer (25 mM Tris-HCl, 150 mM KCl and 1 mM MgCl<sub>2</sub>, pH 7.5) and incubated at 37°C for 1 h. Then the reaction mixture was added to the master mix containing TRAP buffer, dNTP, primers (TS primer, reverse primer, K1 primer), TSK1 DNA template and Taq DNA polymerase. After that, the samples were allowed to incubate at 30°C for 30 min for extension followed by 30-cycle PCR reaction. The extended telomerase products are amplified by PCR using the TS primer and reverse primer (RP), generating a ladder of products with 6 base increments starting at 50 nucleotides: 50, 56, 62, 68, etc. TS plus five telomeric repeats (50 bp) are normally seen as the smallest TRAPEze product using this kit. Smaller products (<50 bp) will appear when the telomerase activity is high. TSK1 template is amplified with TS and K1 primer as a 36-bp internal control to monitor PCR inhibition and inhibit false-negative results. Reaction products were run on an 8% native PAGE and stained with SYBR gold.

**Dual luciferase reporter gene assay.** Firefly/Renilla dual luciferase reporter vector, psiCHECK-2 was used in this assay. Wildtype and mutant *hTERC D-G4* DNA sequences were inserted into the 5' terminal of Renilla luciferase gene at the NheI restriction enzyme site by Genewiz. Wildtype and mutant reporter plasmids were mixed with 0, 50 and 100 nM *cycL-Apt.4-1c* or *cycD-Apt.4-1c* and transfected into HEK293T cells (cell line authenticated and tested without mycoplasma contamination) in 96-well black-wall optical plates using Lipofectamine<sup>®</sup> 2000 with 10 ng plasmids each well. The DMEM medium (Gibco) supplemented with 10% heat-inactivated fetal bovine serum (Gibco) was changed to fresh medium after 24 h of transfection, and cells were incubated for another 24 h. Then luciferase reporter gene assay was conducted using Dual-Luciferase Reporter Assay kit according to the manufacturer's manual. Luciferase activities were recorded by Molecular Devices SpectraMax ID5 Microplate Reader. The intensity of firefly luciferase is used as an internal control. The luciferase activity ratio of Renilla to firefly was calculated for data analysis. All the measurements were performed with four replicates and the standard deviation was plotted as the error bar. The significance level of samples was evaluated using P-value obtained from two-tailed unpaired Student's t tests.

**Total RNA extraction and qRT-PCR test.** The transfection and cell incubation processes are the same as mentioned above for reporter gene assay. After pelleting cells, total RNA was extracted and purified using RNase Plus Mini Kit following the manufacturer's manuals. The concentrations of total RNA samples were detected by NanoDrop spectrophotometer (Thermo Fisher Scientific, USA). Then 100 ng of total RNA was reverse transcribed to cDNA using SuperScript III reverse transcriptase and random primers. After that, qRT-PCR tests for Firefly and Renilla mRNA were conducted, respectively with SsoAdvanced Universal SYBR Green Supermix and corresponding primers using a Bio-Rad CFX96 Touch<sup>™</sup> Real-Time PCR Detection System (USA). All the samples were performed with three replicates and the standard deviation was plotted as the er-

ror bar. The significance level of samples was evaluated using P-value obtained from two-tailed unpaired Student's *t* tests.

## RESULTS

### Design of linear L-RNA aptamer construct and click cyclization

Linear L-Apt.4-1c is a 25-nt long L-RNA oligonucleotide sequence (24), folding into a hairpin structure with 5 base pairs in stem and 15 bases in loop according to Mfold RNA secondary structure prediction (Figure 1) (40). To generate the circular L-RNA aptamer (cycL-Apt.4-1c in this case), we have designed 5'-hexynyl-L-(rArA) and 3'-azide-L-(rArA) to append to the 5' and 3' end of the linear L-Apt.4-1c, where the 5'-hexynyl group contains a 5' terminal alkyne group (Figure 1). The 5' alkyne and 3' azide chemical moieties provide the essential functional groups for the Copper(I)-catalyzed azide-alkyne cycloaddition (CuAAC) (38,39), whereas the incorporation of the extra two L-rAs at the 5' and 3' end sequence of the L-Apt.4-1c provide flexibility during intramolecular click reaction and minimize the effect of the formed triazole unit on the RNA secondary structure of cycL-Apt.4-1c (Supplementary Table S1). In the presence of ascorbic acid, Cu(II) in Cu(II)-TBTA is reduced to Cu(I) and catalyze the intramolecular click chemistry ligation between 5'-alkyne and 3'-azide of the linear precursor, producing the cyclized L-RNA aptamer (Figure 1).

### Optimization of click reaction conditions for L-RNA aptamer cyclization

To improve the efficiency of click cyclization, we first optimized the reaction conditions including the concentration of Cu(II)-TBTA and ascorbic acid (AA), reaction time, reaction temperature, and post-reaction processing (Supplementary Figures S1–S4). Under optimal conditions, cycL-Apt.4-1c was synthesized and purified by Zymo-Spin IC Columns. Then the reaction products were analyzed on denaturing polyacrylamide gel (PAGE) with SYBR Gold staining. As shown in Figure 2, when the cyclization reaction was carried out without Cu(II)-TBTA or AA, the reaction product migrated similarly to the linear control, suggesting that only linear substrate was present in the product. In the presence of both Cu(II)-TBTA and AA, Cu(II) was reduced to Cu(I) by AA and worked as a catalyst for click reaction. A new band was observed to migrate faster than the linear form, which we referred as circular form (Figure 2, lane 4). The faster migration of circular form compared to linear form is not uncommon, and likely caused by its more compact structure after cyclization (36,37,41). Importantly, we found no evidence of slower migration band above the linear form band that may indicate intermolecular click reaction caused by two linear L-Apt.4-1c (Figure 2), suggesting that our rational aptamer construct design and optimized click reaction conditions favor intramolecular cyclization. The linear precursor and cyclization products were further characterized by ESI-MS (Supplementary Figures S5 and S6). The observed mass in mass spectrum (9956.0) of cycL-Apt.4-1c matches the calculated mass

(9955.16) of intramolecular cyclization product (Supplementary Figure S6). The linear form was cyclized to the circular form with approximately 95% efficiency (Figure 2, lane 4), while omitting any of the key components in the reaction resulted in no cyclization (Figure 2, lanes 1–3). Overall, these results support our hypothesis that through rational design of sequence and incorporation of new chemical moieties, L-RNA aptamer can be intramolecularly cyclized using click reaction quantitatively.

### Characterization of secondary structure and target binding affinity of circular L-RNA aptamer

Using a series of biophysical, biochemical and mutagenesis experiments, L-Apt.4-1c was reported by us to adopt a stem-loop structure containing an rG4 motif under physiological-relevant conditions (24). To examine whether the additional triazole group and sequences affect the secondary structure of the cycL-Apt.4-1c, firstly we conducted the G4 ligand enhanced fluorescence assay using Thioflavin T (ThT), one of the well-studied G4 fluorescent turn-on ligands (42). Given that the formation of G4 structure is highly dependent on cations in the order of  $K^+ > Na^+ > Li^+$  (25), we performed fluorescence measurements of cycL-Apt.4-1c with ThT in two different buffers containing either 150 mM  $K^+$  (G4 stabilizing) or  $Li^+$  (G4 non-stabilizing), respectively. A 3-fold fluorescence enhancement in the presence of  $K^+$  than  $Li^+$  conditions was detected (Figure 3A), which verified the formation of rG4 in cycL-Apt.4-1c. Compared with the 2.2-fold fluorescence enhancement of linear L-Apt.4-1c in the two conditions (Supplementary Figure S7), cycL-apt.4-1c is more likely to form rG4 structure after cyclization. Then we investigated the conformation behavior of cycL-Apt.4-1c using CD measurements. Under both  $K^+$  and  $Li^+$  conditions, the CD spectrum of cycL-Apt.4-1c showed a positive band at 236 nm and a negative band at 266 nm (Figure 3B), similarly to L-Apt.4-1c (Supplementary Figure S8), suggesting the formation of left-handed parallel G-quadruplex. These results clearly verified that cyclization did not affect the folding topology of L-Apt.4-1c.

To evaluate the effect of cyclization on target recognition ability, we performed the binding of cycL-Apt.4-1c to *hTERC* D-rG4 target using electrophoretic mobility shift assay (EMSA) (Figure 3C and D, Supplementary Figure S9). The dissociation constant ( $K_d$ ) was determined to be  $7.76 \pm 0.95$  nM for cycL-Apt.4-1c, which is approximately 10 times lower than linear L-Apt.4-1c (Supplementary Figure S10) (24). To corroborate the result, we also used microscale thermophoresis (MST) assay and found that the  $K_d$  was determined to be  $6.24 \pm 1.65$  nM (Supplementary Figure S11), which is consistent with the EMSA result (Figure 3C and D). We reasoned that the 10-fold improvement in binding affinity (lower  $K_d$  value) for circular form is caused by its improved conformational stability as compared to the linear form, as chemical denaturation experiment using urea suggested that the circular form is predominately in the functional folded state (Supplementary Figure S12). As shown in Supplementary Figure S12, in the native state without urea, cycL-Apt.4-1c is in a unitary folded conformation and migrated as a single band (Supplementary Figure S12B, lane 1), while two bands were displayed for L-

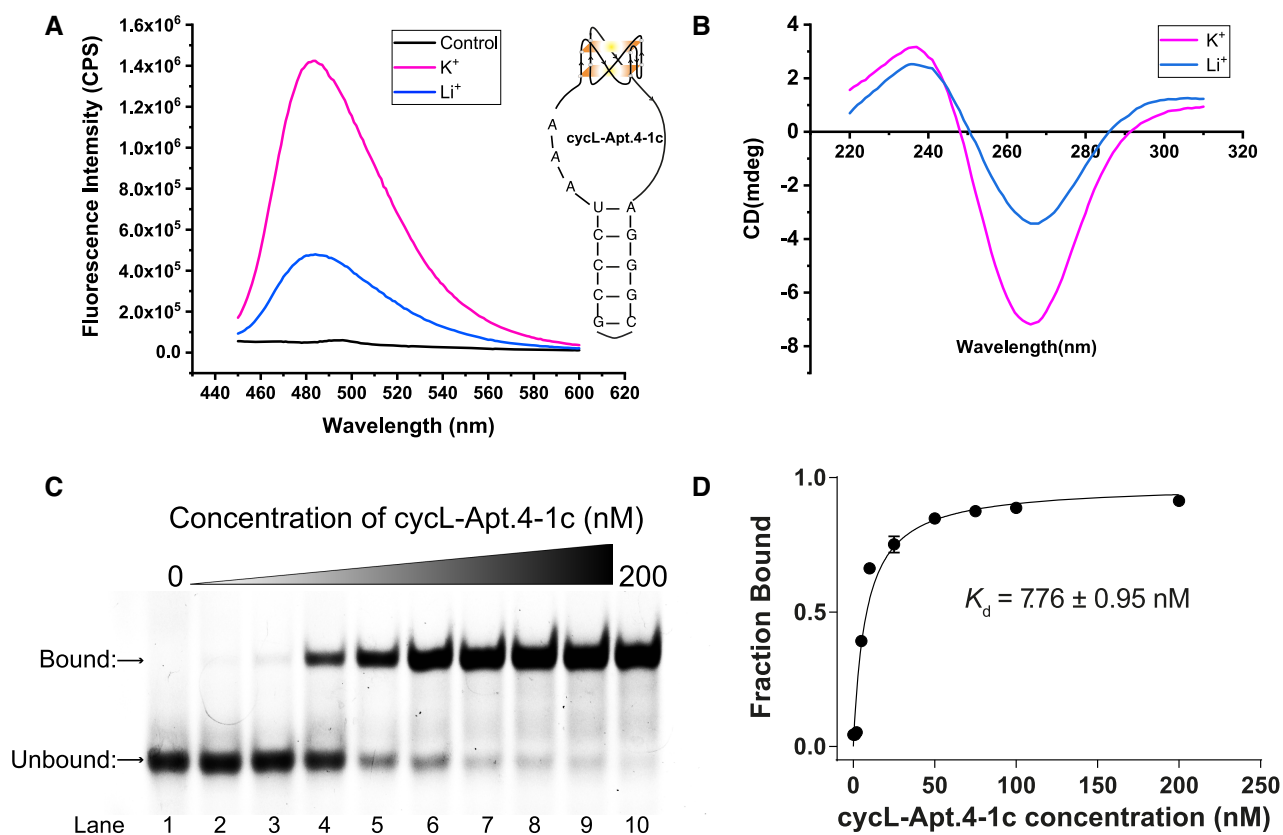


**Figure 3.** G-quadruplex structure characterization of cycl-L-Apt.4-1c and binding affinity test to *hTERC* D-rG4 target. (A) Fluorescence emission spectra of G4-specific ligand ThT (2  $\mu$ M) with cycl-L-Apt.4-1c (300 nM) under 150 mM KCl (pink) and LiCl (blue) condition. ThT without cycl-L-Apt.4-1c is used as control (black). The K<sup>+</sup>-dependent enhanced fluorescence in ThT supports the formation of rG4 in cycl-L-Apt.4-1c. (B) CD spectrum of 500 nM cycl-L-Apt.4-1c under 150 mM KCl and LiCl condition. CD spectra suggests the formation of a left-handed parallel G-quadruplex structure in cycl-L-Apt.4-1c. (C) EMSA shows the binding between cycl-L-Apt.4-1c and FAM-*hTERC* D-rG4 target. With increasing concentration of cycl-L-Apt.4-1c (lanes 1–10: 0, 1, 2, 5, 10, 25, 50, 75, 100, 200 nM), the unbound band intensity decreases and the bound band intensity increases, indicates the interaction between the FAM-*hTERC* D-rG4 and cycl-L-Apt.4-1c. (D) Binding curve of FAM-*hTERC* D-rG4 against cycl-L-Apt.4-1c based on data from (C). The  $K_d$  is determined to be  $7.76 \pm 0.95$  nM. The error bar represents the standard deviation of three independent replicates.

Apt.4-1c (Supplementary Figure S12A, lane 1), suggesting a mixed conformation occurring for linear form. With increasing concentrations of urea to denature secondary structures, more and more L-Apt.4-1c went to the lower band and finally the upper band disappeared, which indicating that the upper and lower bands are folded structure and non-folded open structures, respectively. Cycl-L-Apt.4-1c maintained stable folded structures in lower concentrations of urea and transformed to non-folded open form only under 5 M urea. Collectively, these results provide strong evidence that cyclization can enhance the conformational stability of linear aptamer, resulting to a higher percentage of functional folded aptamers for target recognition, thus leading to strong binding affinity of cycl-L-Apt.4-1c to *hTERC* D-rG4 target observed. Furthermore, the increased binding affinity of cycl-L-Apt.4-1c can be explained by Gibbs free energy change of aptamer after cyclization, which is discussed in Note S1.

#### Characterization of target binding specificity and stability of circular L-RNA aptamer

To investigate the impact of cyclization on target binding specificity, we conducted the binding of cycl-L-Apt.4-1c to

nine different targets that cover different structural motifs in nucleic acids, including single-stranded polyA/C/U RNAs, hairpin DNA/RNA, *hTERC* D-rG4 mutants, and DNA G4 (dG4) sequences, and none of them showed binding to cycl-L-Apt.4-1c (Figure 4). Notably, while the *hTERC* D-rG4 showed a weak binding to linear L-Apt.4-1c with a  $K_d$  value of  $315 \pm 81$  nM previously (24), no observable binding was found to cycl-L-Apt.4-1c, suggested an improvement in binding selectivity (Figure 4). These results revealed that the L-RNA aptamer cyclization and the additional sequence in cycl-L-Apt.4-1c did not produce new binding motifs for non-target structural motifs, and the much stronger binding affinity of cycl-L-Apt.4-1c to *hTERC* D-rG4 target also promotes its binding specificity to some extent, as evident by the reduced binding affinity to *hTERC* D-dG4 non-target (Supplementary Figure S13).

Having demonstrated the ideal stability of L-Apt.4-1c in nuclease-containing and complex conditions (Supplementary Figure S14), we then assessed the stability of cycl-L-Apt.4-1c in different biological conditions. We initially tested its stability in ribonuclease A (RNase A), and found that no degradation of the cycl-L-Apt.4-1c was observed within the two hour reaction window (Figure 5). Other nuclease-containing conditions, such as in fetal bovine

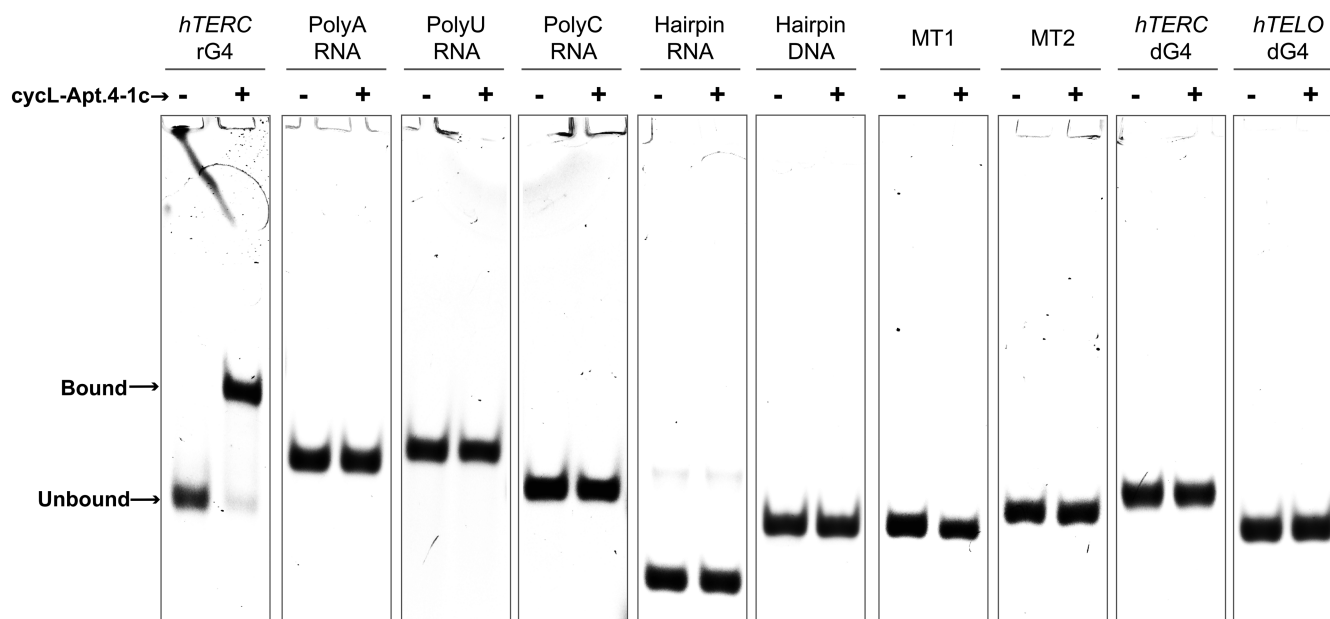


**Figure 4.** cycl-L-Apt.4-1c exhibits strong binding specificity toward *hTERC* D-rG4. Native gel shows that among the 10 constructs tested, only FAM-*hTERC* D-rG4 interacted with cycl-L-Apt.4-1c and caused gel shift, whereas the other constructs such as single-stranded polyA/U/C RNAs, hairpin RNA/DNA, *hTERC* rG4 mutants (MT1 and MT2), and dG4s have no observable binding to cycl-L-Apt.4-1c. The concentration of cycl-L-Apt.4-1c used is 100 nM.

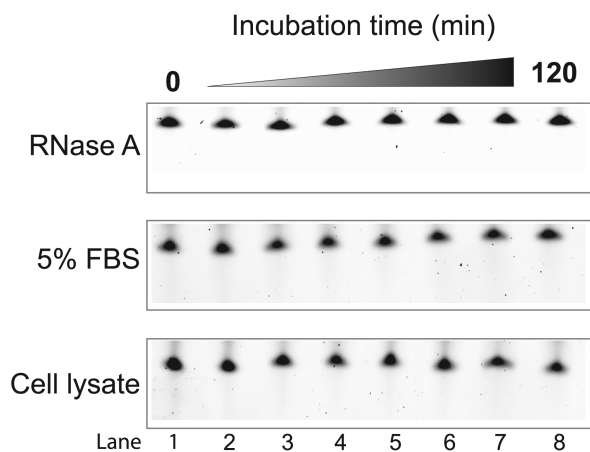


**Figure 5.** Cycl-L-Apt.4-1c displays high stability in nuclease-containing and complex conditions. Denaturing PAGE gel shows that cycl-L-Apt.4-1c is highly stable in RNase A, FBS, and cell lysate conditions. No degradation was observed from 0–120 min treatment (lanes 1–8), indicating that the circular L-RNA aptamer is nuclease-resistant and biostable under these complex conditions.

serum (FBS) and cell lysate conditions were also carried out similarly, and again no degradation of the cycl-L-Apt.4-1c was observed, which was attributed to the nuclease-resistant property of L-RNA. This also suggested that the additional triazole-containing linker is biostable and aptamer remains in circular form in biological conditions in the reactions (Figure 5). As a control, we measured the stability of cycl-L-Apt.4-1c in strong alkaline conditions, to demonstrate that cycl-L-Apt.4-1c can indeed be degraded under very high pH (i.e. pH 13 in our case) owing to the base-catalyzed hydrolysis (Supplementary Figure S15). Taken together, the results

above highlight the enhancement of cycl-L-Apt.4-1c in binding selectivity toward its target, as well as its strong stability in nuclease-containing conditions, making it suitable for different downstream applications in more complex conditions.

#### Applications of circular L-RNA aptamer in controlling RNA–protein interaction and gene activity in vitro and in vivo

To showcase the potential applications of circular L-RNA aptamer, we next studied the utility of cycl-L-Apt.4-1c in three important ways. First, we assessed its ability to inhibit the rG4-protein interaction. RNA helicase associated with AU-rich elements (RHAU), or often known as DHX36, was reported to associate with *hTERC* D-rG4 to interfere telomerase activity (43), and was therefore used in this inhibition assay. The result showed that by increasing the concentration of cycl-L-Apt.4-1c, the *hTERC* D-rG4-DHX36 complex was found to be weaker, while the rG4-cycl-L-Apt.4-1c complex was found to be stronger (Figure 6A), indicating that the cycl-L-Apt.4-1c can competitively displace the *hTERC* D-rG4-DHX36 complex. The half maximal inhibitory concentration (IC<sub>50</sub>) value was determined to be  $11.45 \pm 1.06$  nM (Figure 6B). The low IC<sub>50</sub> value arises from the strong binding affinity of cycl-L-Apt.4-1c to *hTERC* D-rG4 (Figure 3C and D), which allows it to dissociate the *hTERC* D-rG4-DHX36 complex effectively.

Second, we examined whether cycl-L-Apt.4-1c can inhibit telomerase activity (Figure 6C). We first tested the telomerase activity of telomerase-positive HEK293T cell by setting up telomerase repeated amplification protocol (TRAP) assay with serial dilutions of HEK293T cell extracts, and observed a cell number-dependent amplification (Supplementary Figure S16). Next, we assessed the inhibition effect of cycl-L-Apt.4-1c on telomerase activity of 293T cell

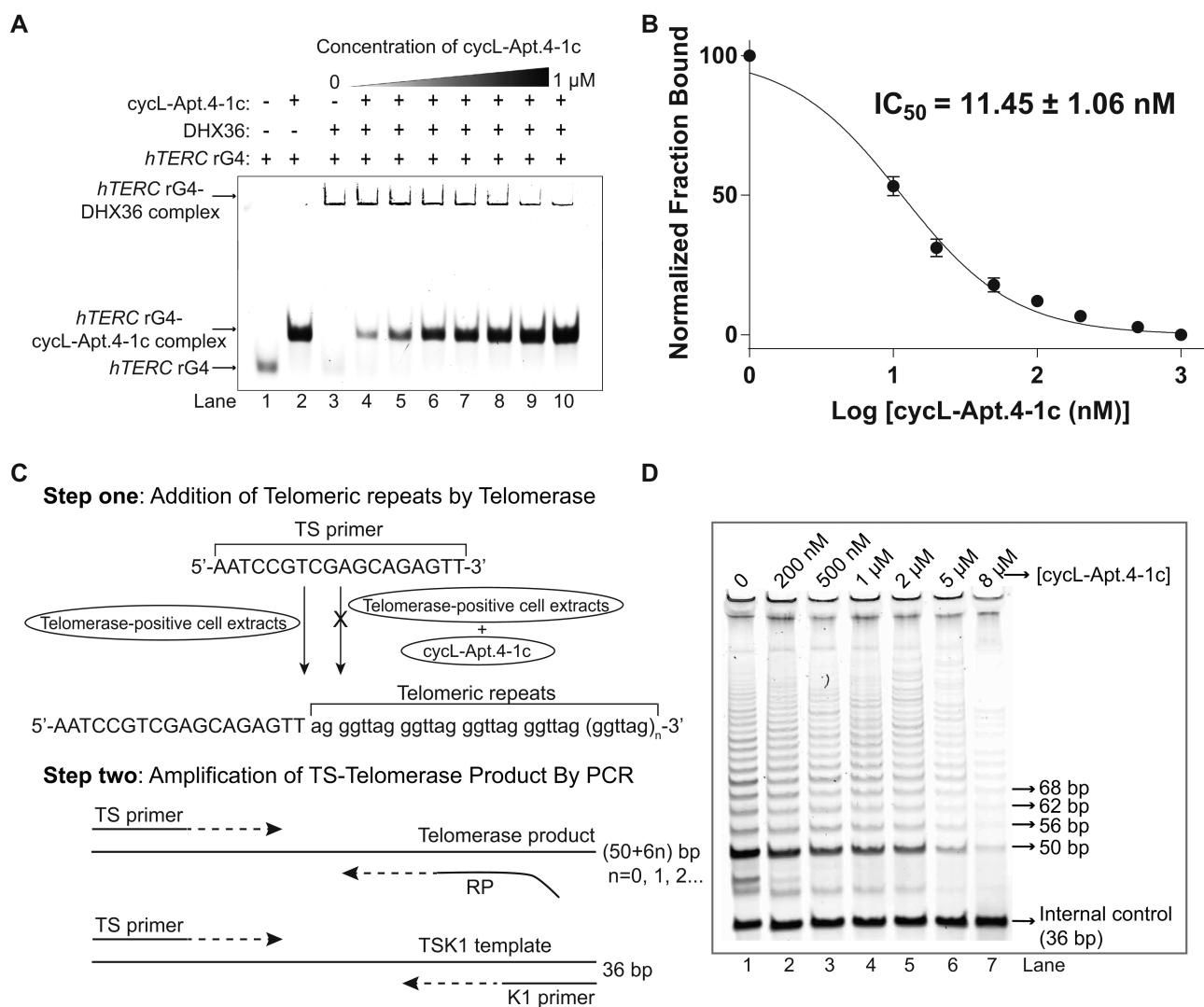


**Figure 6.** cycl-Apt.4-1c can inhibit *hTERC* D-rG4-DHX36 interaction and suppress telomerase activity. (A) EMSA shows that the binding of DHX36 and FAM-*hTERC* D-rG4 is inhibited by cycl-Apt.4-1c (lanes 3-10: 0, 10, 20, 50, 100, 200, 500, 1000 nM). (B) Inhibition curve of cycl-Apt.4-1c on *hTERC* D-rG4-DHX36 complex generated from data in (A). IC<sub>50</sub> was determined to be 11.45 ± 1.06 nM. The error bar represents the standard deviation of three independent replicates. (C) The workflow of the TRAP assay. Cycl-Apt.4-1c is pre-incubated with telomerase-positive HEK293T cell extracts before TRAP assay. TSK1 templates is amplified with TS and K1 primer as a 36 bp internal control. The telomerase product is amplified by TS primer and reverse primer (RP) to generate 50 bp + 6n (n = 0, 1, 2, ...) telomerase products. (D) TRAP assay shows that the telomerase activity is suppressed by cycl-Apt.4-1c treatment in HEK293T cell lysate. With increasing concentration of cycl-Apt.4-1c added (lanes 1-7: 0, 200 nM, 500 nM, 1  $\mu$ M, 2  $\mu$ M, 5  $\mu$ M, 8  $\mu$ M), the telomerase products are weaker (lanes 2-7).

extracts, and found that the intensity of telomerase products dropped with increasing concentrations of cycl-Apt.4-1c (Figure 6D), which suggests that cycl-Apt.4-1c can bind to *hTERC* D-rG4 in cell extracts and suppress telomerase activity effectively. CycD-Apt.4-1c and another stem-loop L-RNA oligo (L-SLRNA), which are unable to bind to *hTERC* D-rG4 (Supplementary Figures S17 and S18), were used as a negative control in the same experimental set up, and no inhibition effect was observed (Supplementary Figures S19 and S20). G4 ligand BRACO-19, which was previously reported by others to reduce telomerase activity (44) and was used as a positive control in the same experimental set up, and inhibition effect was observed (Supplementary Figure S21). This result provides substantial evidence the effect of cycl-Apt.4-1c reported herein is G4-specific.

Last, we investigated whether cycl-Apt.4-1c can be used to control gene activity in cells. To do so, the *hTERC* wildtype dG4 and mutant dG4 motifs were incorporated into the 5' untranslated region (5'UTR) of the Renilla luciferase gene reporter plasmid constructs separately (Figure 7A), and the dual luciferase gene reporter assays were conducted. Our data showed that in the absence of cycl-Apt.4-1c aptamer in both constructs, the wildtype construct has approximately 2.2 times lower luciferase activity than the mutant construct (Figure 7B, C), which suggests that *hTERC* D-rG4 sequence can fold into rG4 in cell and negatively regulates the gene expression. The rG4-mediated gene suppression is consistent with other 5'UTR rG4s reported elsewhere (45,46). Notably, the luciferase activity of the wildtype construct, but not the mutant con-

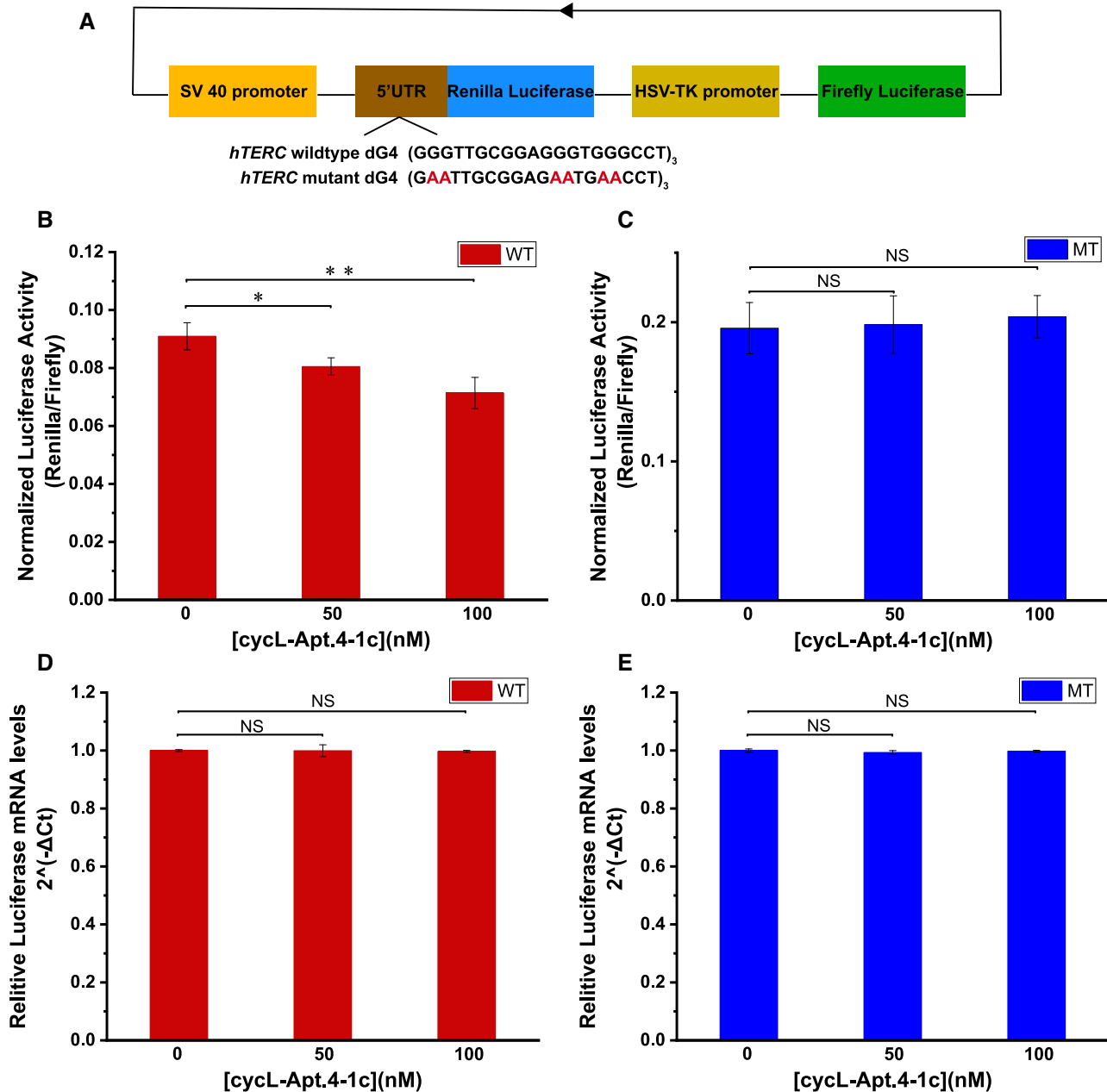


**Figure 7.** cycL-Apt.4-1c can regulate gene activity in cells. (A) Schematic illustration of the design of luciferase reporter plasmids. The *hTERC* G4 wildtype or mutant DNA sequence is inserted into the 5'UTR of Renilla luciferase. The firefly luciferase is used as internal control to account for transfection variation. (B) Normalized luciferase activity of cells transfected with *hTERC* dG4 wildtype plasmid (WT) and cycL-Apt.4-1c. With increasing cycL-Apt.4-1c (0, 50, 100 nM) treatment in cells, the luciferase activity level of the WT construct decreases. (C) Normalized luciferase activity of cells transfected with *hTERC* dG4 mutant plasmid (MT) and cycL-Apt.4-1c (0, 50 nM, 100 nM). No significant changes are observed. The error bar represents the standard deviation of four independent replicates. \* $P < 0.05$ , \*\* $P < 0.01$ , NS: not significant. (D) Relative luciferase mRNA expression levels of wildtype *hTERC* dG4 plasmid (WT) with addition of 0 nM, 50 nM and 100 nM cycL-Apt.4-1c. (E) Relative luciferase mRNA expression levels of mutant *hTERC* dG4 plasmid (MT) with addition of 0, 50 and 100 nM cycL-Apt.4-1c. The error bar represents the standard deviation of three independent replicates. NS: not significant.

struct, were lowered significantly with cycL-Apt.4-1c addition (Figure 7B, C), indicated the suppression in gene expression. As a control, cycD-Apt.4-1c were added instead of cycL-Apt.4-1c, and no significant difference was observed (Supplementary Figure S22). To study whether cycL-Apt.4-1c regulates the gene expression on transcriptional and/or translational level, the mRNA level of Firefly

and Renilla luciferase was also measured by quantitative reverse transcriptase-polymerase chain reaction (qRT-PCR), and no significant difference was observed (Figure 7D, E), highlighting that cycL-Apt.4-1c did not interfere with the transcription and regulate gene expression at translational level by interacting with *hTERC* D-rG4. This result also supported with the fact that cycL-Apt.4-1c interacts only

with D-*hTERC* rG4, but not D-*hTERC* dG4 (Figure 4). Overall, these data demonstrate novel applications of circular cycL-Apt.4-1c in controlling RNA–protein interaction, and gene activity including telomerase activity and gene expression.

## DISCUSSION

In this study, we have demonstrated for the first time the successful development of unnatural, circular L-RNA aptamers. While cyclization of linear D-aptamers and application of circular D-aptamers have been reported in the past (33,37,47,48), to the best of our knowledge, there is no report that shows the strategy and feasibility to synthesize circular L-aptamer. Besides that, through our systematic optimization of the click reaction, we were able to achieve almost quantitative intramolecular ligation, with approximately 95% yield (Figure 2). Another key feature is that no intermolecular ligation was observed in our optimized click reaction, which simplify the post-click reaction cleanup steps and allow the circular L-RNA aptamer to be readily used for aptamer characterization and downstream applications. Importantly, the cyclization not only did not impart any undesirable effect in terms of the secondary structure folding of the circular L-RNA aptamer, as evident by the proper folding of rG4 motif in our data (Figure 3A, B), but also helps to improve the binding affinity and selectivity as compared to the linear L-aptamer counterpart (Figures 3C, D and 4). Based on our data, we reasoned that the enhancement in target binding affinity and selectivity for circular L-RNA aptamer as compared to the linear L-RNA aptamer counterpart is likely caused by the increased conformational stability mediated by the aptamer cyclization (Supplementary Figure S12). This general method allows more functional fold of the L-aptamer to be populated under the reaction conditions to recognize the desired target, providing a simple and robust strategy to potentially apply to other L-aptamer system to recognize diverse target of interest.

The nuclease-resistance and biostability of unnatural L-RNA aptamer enable it to be promising tool for applications in more complex conditions, such as nuclease-containing conditions or *in vivo* applications. Here, we reported for the first time that through targeting rG4 structure motif of *hTERC* RNA, the circular L-RNA aptamer we developed, cycL-Apt.4-1c can be employed to control gene functions such as telomerase activity and gene expression in cells. We wish to note that linear L-RNA aptamers that target rG4 have been developed and applied to disrupt rG4-peptide/protein interactions by us recently (23,24), however, in those studies the experiments were performed under standard buffer conditions (23), and its performance dropped drastically in the presence of nuclease-containing or cell lysate environment (24), limiting its applications in complex environment. On the other hand, it should be noted that aptamer cyclization cannot always provide improved biological results. Riccardi and co-authors reported a cyclized thrombin-binding aptamer (cycTBA) by cyclizing a 15-mer G-rich thrombin-binding DNA aptamer (TBA) using copper(I)-assisted azide-alkyne cycloaddition (47). The cyclized DNA aptamer showed increased stabil-

ity and serum resistance, but with much reduced thrombin inhibition compared to unmodified TBA owing to its lower binding affinity to thrombin. Riccardi concluded that this probably results from the increased rigidity of the aptamer G4 core after cyclization. Thus, they optimized the length of connecting linker from 20 atoms to 48 atoms to achieve higher structural flexibility (48). Finally, the best candidate was proved to be cycTBA II with a 30 atom-long linker, which showed increased structure stabilization and nuclease resistance, as well as improved binding affinity to thrombin and anticoagulant activity. This suggested that the best compromise between stabilizing the initial aptamer core structure and maintaining structural flexibility for improved target recognition can be realized by optimizing the length or chemical structure of connecting linker.

In this work, we rationally designed the connecting linker by adding additional sequences with chemical moieties to the linear L-Apt.4-1c. Before cyclizing L-Apt.4-1c, we optimized the sequence using D-Apt.4-1c and *hTERC* L-rG4 as target. Three D-RNA sequences with different number of terminal D-rAs were tested for D-Apt.4-1c cyclization (Supplementary Table S1). Based on the cyclization and binding results (Supplementary Figures S23–S26), we selected the sequence with connecting linkers of 5'-hexynyl-rArA and 3'-azide-rArA and converted it to L-RNA sequence for cyclization. The developed circular L-RNA aptamer, a new class of modified aptamer is stable in diverse conditions including RNase A, FBS and cell lysate (Figure 5), and even at high pH such as pH 11 for an extended reaction time period (Supplementary Figure S15). Notably, we illustrated that cycL-Apt.4-1c, besides having the ability to dissociate *hTERC* D-rG4-DHX36 complex *in vitro*, can be employed in cell lysate and *in vivo* to control gene activity effectively (Figures 6 and 7). It will be interesting in the future to detect telomerase activity in cells and apply cycL-Apt.4-1c to investigate telomere, telomerase, and cancer biology. Overall, our proof-of-concept study and findings here should open up new avenues for targeting RNA structure via circular L-RNA aptamer to regulate gene functions, which will provide valuable insights into the further development of modified aptamer-mediated tools for gene regulation and other biological applications.

## CONCLUSION

In sum, through rational design and incorporation of chemical moieties and sequences into linear L-RNA aptamer, we have reported a novel approach to generate the first circular L-RNA aptamer, cycL-Apt.4-1c. Notably, we demonstrated its superior binding affinity and specificity to its linear counterpart, and highlighted its utility through multiple *in vitro* and *in vivo* applications. These results clearly illustrated that the head-to-tail intramolecular cyclization can be a general and robust way to strengthen the performance of L-RNA aptamer in standard buffer or complex conditions that are of physiological relevance *in vitro* or in cells. Furthermore, our general strategy should be applicable for any L-RNAs to expand their functional complexity and diversity for different applications.

**DATA AVAILABILITY**

The data generated during all experiments is available from the author upon reasonable request.

**SUPPLEMENTARY DATA**

Supplementary Data are available at NAR Online.

**ACKNOWLEDGEMENTS**

We thank Dr Mubarak I. Umar for the discussion.

**FUNDING**

Shenzhen Basic Research Project [JCYJ20180507181642 811]; Research Grants Council of the Hong Kong SAR, China Projects [CityU 11100421, CityU 11101519, CityU 11100218, N\_CityU110/17, CityU 21302317]; Croucher Foundation Project [9500030, 9509003]; State Key Laboratory of Marine Pollution Director Discretionary Fund; City University of Hong Kong projects [6000711, 7005503, 9667222, 9680261] to C.K.K.. Funding for open access charge: Research Grants Council of the Hong Kong SAR [CityU 11101519].

*Conflict of interest statement.* None declared.

**REFERENCES**

- Dunn, M.R., Jimenez, R.M. and Chaput, J.C. (2017) Analysis of aptamer discovery and technology. *Nat. Rev. Chem.*, **1**, 0076.
- Rothlisberger, P. and Hollenstein, M. (2018) Aptamer chemistry. *Adv. Drug Deliver. Rev.*, **134**, 3–21.
- Ozer, A., Pagano, J.M. and Lis, J.T. (2014) New technologies provide quantum changes in the scale, speed, and success of SELEX methods and aptamer characterization. *Mol. Ther.-Nucl. Acids*, **3**, e183.
- Keefe, A.D., Pai, S. and Ellington, A. (2010) Aptamers as therapeutics. *Nat. Rev. Drug Discov.*, **9**, 537–550.
- Li, L., Xu, S., Yan, H., Li, X., Yazd, H.S., Li, X. and Tan, W. (2021) Nucleic acid aptamers for molecular diagnostics and therapeutics: advances and perspectives. *Angew. Chem. Int. Ed.*, **60**, 2221–2231.
- Deng, C., Chen, J., Nie, L., Nie, Z. and Yao, S. (2009) Sensitive bifunctional aptamer-based electrochemical biosensor for small molecules and protein. *Anal. Chem.*, **81**, 9972–9978.
- Zhang, Y., Lai, B.S. and Juhas, M. (2019) Recent advances in aptamer discovery and applications. *Molecules*, **24**, 941.
- Tsui, N.B., Ng, E.K. and Lo, Y.D. (2002) Stability of endogenous and added RNA in blood specimens, serum, and plasma. *Clin. Chem.*, **48**, 1647–1653.
- Lakhin, A.V., Tarantul, V.Z. and Gening, L.V. (2013) Aptamers: problems, solutions and prospects. *Acta Naturae*, **5**, 34–43.
- Dunn, M.R., McCloskey, C.M., Buckley, P., Rhea, K. and Chaput, J.C. (2020) Generating biologically stable TNA aptamers that function with high affinity and thermal stability. *J. Am. Chem. Soc.*, **142**, 7721–7724.
- Maio, G., Enweronye, O., Zumrut, H.E., Batool, S., Van, N. and Mallikaratchy, P. (2017) Systematic optimization and modification of a DNA aptamer with 2'-O-Methyl RNA analogues. *ChemistrySelect*, **2**, 2335–2340.
- Hoshino, H., Kasahara, Y., Kuwahara, M. and Obika, S. (2020) DNA polymerase variants with high processivity and accuracy for encoding and decoding locked nucleic acid sequences. *J. Am. Chem. Soc.*, **142**, 21530–21537.
- Biondi, E. and Benner, S.A. (2018) Artificially expanded genetic information systems for new aptamer technologies. *Biomedicines*, **6**, 53.
- Liao, J.Y., Bala, S., Ngor, A.K., Yik, E.J. and Chaput, J.C. (2019) P(V) reagents for the scalable synthesis of natural and modified nucleoside triphosphates. *J. Am. Chem. Soc.*, **141**, 13286–13289.
- Olea, C. Jr, Weidmann, J., Dawson, P.E. and Joyce, G.F. (2015) An L-RNA aptamer that binds and inhibits RNase. *Chem. Biol.*, **22**, 1437–1441.
- Rangel, A.E., Chen, Z., Ayele, T.M. and Heemstra, J.M. (2018) In vitro selection of an XNA aptamer capable of small-molecule recognition. *Nucleic Acids Res.*, **46**, 8057–8068.
- Meek, K.N., Rangel, A.E. and Heemstra, J.M. (2016) Enhancing aptamer function and stability via in vitro selection using modified nucleic acids. *Methods*, **106**, 29–36.
- Kluszmann, S., Nolte, A., Bald, R., Erdmann, V.A. and Furste, J.P. (1996) Mirror-image RNA that binds D-adenosine. *Nat. Biotechnol.*, **14**, 1112–1115.
- Nolte, A., Kluszmann, S., Bald, R., Erdmann, V.A. and Furste, J.P. (1996) Mirror-design of L-oligonucleotide ligands binding to L-arginine. *Nat. Biotechnol.*, **14**, 1116–1119.
- Sczepanski, J.T. and Joyce, G.F. (2013) Binding of a structured D-RNA molecule by an L-RNA aptamer. *J. Am. Chem. Soc.*, **135**, 13290–13293.
- Sczepanski, J.T. and Joyce, G.F. (2015) Specific inhibition of microRNA processing using L-RNA aptamers. *J. Am. Chem. Soc.*, **137**, 16032–16037.
- Kabza, A.M. and Sczepanski, J.T. (2017) An L-RNA Aptamer with expanded chemical functionality that inhibits microRNA biogenesis. *Chembiochem*, **18**, 1824–1827.
- Chan, C.Y. and Kwok, C.K. (2020) Specific binding of a D-RNA G-quadruplex structure with an L-RNA aptamer. *Angew. Chem. Int. Ed.*, **132**, 5331–5335.
- Umar, M.I. and Kwok, C.K. (2020) Specific suppression of D-RNA G-quadruplex-protein interaction with an L-RNA aptamer. *Nucleic Acids Res.*, **48**, 10125–10141.
- Lyu, K., Chow, E.Y., Mou, X., Chan, T.F. and Kwok, C.K. (2021) RNA G-quadruplexes (rG4s): genomics and biological functions. *Nucleic Acids Res.*, **49**, 5426–5450.
- Tassinari, M., Richter, S.N. and Gandellini, P. (2021) Biological relevance and therapeutic potential of G-quadruplex structures in the human noncoding transcriptome. *Nucleic Acids Res.*, **49**, 3617–3633.
- Kharel, P., Becker, G., Tsvetkov, V. and Ivanov, P. (2020) Properties and biological impact of RNA G-quadruplexes: from order to turmoil and back. *Nucleic Acids Res.*, **48**, 12534–12555.
- Varshney, D., Spiegel, J., Zyner, K., Tannahill, D. and Balasubramanian, S. (2020) The regulation and functions of DNA and RNA G-quadruplexes. *Nat. Rev. Mol. Cell. Biol.*, **21**, 459–474.
- Young, B.E., Kundu, N. and Sczepanski, J.T. (2019) Mirror-image oligonucleotides: history and emerging applications. *Chemistry*, **25**, 7981–7990.
- Zhong, W. and Sczepanski, J.T. (2019) A Mirror image fluorogenic aptamer sensor for live-cell imaging of microRNAs. *ACS Sens.*, **4**, 566–570.
- Young, B.E., Kundu, N. and Sczepanski, J.T. (2019) Mirror-image oligonucleotides: history and emerging applications. *Chemistry*, **25**, 7981–7990.
- Eaton, B.E., Gold, L. and Zichi, D.A. (1995) Let's get specific: the relationship between specificity and affinity. *Chem. Biol.*, **2**, 633–638.
- Kuai, H., Zhao, Z., Mo, L., Liu, H., Hu, X., Fu, T., Zhang, X. and Tan, W. (2017) Circular bivalent aptamers enable *in vivo* stability and recognition. *J. Am. Chem. Soc.*, **139**, 9128–9131.
- Andrusishina, I.N. (2010) Diagnostic values of calcium and magnesium forms determined in human serum and saliva. *J. Elementol.*, **15**, 425–433.
- Petkovic, S. and Muller, S. (2015) RNA circularization strategies *in vivo* and *in vitro*. *Nucleic Acids Res.*, **43**, 2454–2465.
- Kiliszek, A., Blaszczyk, L., Kierzek, R. and Rypniewski, W. (2017) Stabilization of RNA hairpins using non-nucleotide linkers and circularization. *Nucleic Acids Res.*, **45**, e92.
- Litke, J.L. and Jaffrey, S.R. (2019) Highly efficient expression of circular RNA aptamers in cells using autocatalytic transcripts. *Nat. Biotechnol.*, **37**, 667–675.
- El-Sagheer, A.H. and Brown, T. (2010) Click chemistry with DNA. *Chem. Soc. Rev.*, **39**, 1388–1405.
- Liu, J., Leonard, P., Muller, S.L., Daniluc, C. and Seela, F. (2018) Nucleoside macrocycles formed by intramolecular click reaction: efficient cyclization of pyrimidine nucleosides decorated with 5'-azido residues and 5-octadiynyl side chains. *Beilstein J. Org. Chem.*, **14**, 2404–2410.

40. Zuker, M. (2003) Mfold web server for nucleic acid folding and hybridization prediction. *Nucleic Acids Res.*, **31**, 3406–3415.
41. Tabak, H.F., Van der Horst, G., Smit, J., Winter, A.J., Mul, Y. and Koerkamp, G.M. (1988) Discrimination between RNA circles, interlocked RNA circles and lariats using two-dimensional polyacrylamide gel electrophoresis. *Nucleic Acids Res.*, **16**, 6597–6605.
42. Umar, M.I., Ji, D., Chan, C.Y. and Kwok, C.K. (2019) G-Quadruplex-based fluorescent turn-on ligands and aptamers: from development to applications. *Molecules*, **24**, 2416.
43. Lattmann, S., Stadler, M.B., Vaughn, J.P., Akman, S.A. and Nagamine, Y. (2011) The DEAH-box RNA helicase RHAU binds an intramolecular RNA G-quadruplex in TERC and associates with telomerase holoenzyme. *Nucleic Acids Res.*, **39**, 9390–9404.
44. Reed, J., Gunaratnam, M., Beltran, M., Reszka, A.P., Vilar, R. and Neidle, S. (2008) TRAP-LIG, a modified telomere repeat amplification protocol assay to quantitate telomerase inhibition by small molecules. *Anal. Biochem.*, **380**, 99–105.
45. Kumari, S., Bugaut, A., Huppert, J.L. and Balasubramanian, S. (2007) An RNA G-quadruplex in the 5'UTR of the NRAS proto-oncogene modulates translation. *Nat. Chem. Biol.*, **3**, 218–221.
46. Jodoin, R., Carrier, J.C., Rivard, N., Bisailon, M. and Perreault, J.P. (2019) G-quadruplex located in the 5'UTR of the BAG-1 mRNA affects both its cap-dependent and cap-independent translation through global secondary structure maintenance. *Nucleic Acids Res.*, **47**, 10247–10266.
47. Riccardi, C., Meyer, A., Vasseur, J.J., Paduano, L., Oliva, R., Petraccone, L. and Montesarchio, D. (2019) Stability is not everything: the case of the cyclisation of a thrombin-binding aptamer. *ChemBioChem*, **20**, 1789–1794.
48. Riccardi, C., Meyer, A., Vasseur, J.J., Krauss, I.R., Paduano, L., Morvan, F. and Montesarchio, D. (2020) Fine-tuning the properties of the thrombin binding aptamer through cyclization: Effect of the 5'-3' connecting linker on the aptamer stability and anticoagulant activity. *Bioorg. Chem.*, **94**, 103379.